Hydrogen-Bonded Monolayers and Interdigitated Multilayers at the Air−Water Interface

Stephen M. Martin,[†] Kristian Kjaer,[‡,⊥] Markus J. Weygand,[‡,∥] Isabelle Weissbuch,[*,§] and Michael D. Ward[*,†,▽]

Department of Chemical Engineering and Materials Science, University of Minnesota, Minneapolis, Minnesota 55455, Department of Materials and Interfaces, The Weizmann Institute of Science, 76100 Rehovot, Israel, and Materials Research Department, Risø National Laboratory, DK 4000, Roskilde, Denmark

Received: November 1, 2005; In Final Form: May 4, 2006

Crystalline monolayers of octadecylsulfonate amphiphiles (C18S) separated by hydrophilic guanidinium (**G**) spacer molecules were formed at the air−water interface at a surface coverage that was consistent with that expected for a fully condensed monolayer self-assembled by hydrogen bonding between the **G** ions and the sulfonate groups. The surface pressure−area isotherms reflected reinforcement of this monolayer by hydrogen bonding between the **G** ions and the sulfonate groups, and grazing incidence X-ray diffraction (GIXD) measurements, performed in-situ at the air−water interface, revealed substantial tilt of the alkyl hydrophobes ($t = 49°$ with respect to the surface normal), which allowed the close packing of the C18 chains needed for a stable crystalline monolayer. This property contrasts with behavior observed previously for monolayers of hexadecylbiphenylsulfonate (C16BPS) and **G**, which only formed crystallites upon compression, accompanied by ejection of the **G** ions from the air−water interface. Upon compression to higher surface pressures, GIXD revealed that the highly tilted (**G**)C18S monolayer crystallites transformed to a self-interdigitated (**G**)C18S crystalline multilayer accompanied by a new crystalline monolayer phase with slightly tilted alkyl chains and disordered sulfonate headgroups. This transformation was dependent on the rate of compression, suggesting kinetic limitations for the "zipper-like" transformation from the crystalline monolayer to the self-interdigitated (**G**)C18S crystalline multilayer.

Introduction

Molecular complexes at the air−water interface consisting of two or more components span a range of architectures (Figure 1). Binary monolayers consisting of two different amphiphiles assembled through specific interactions at the air−water interface and stabilized by hydrophobe-hydrophobe contacts (Figure 1a) have been reported.[1,2] Binary complexes of a different kind in which molecules bind to amphiphiles from beneath the air−water interface or insert at the air−water interface also have been reported (Figure 1b−d).[3−8] Certain examples of configurations a, b, and d in Figure 1 have been proven crystalline by grazing incidence X-ray diffraction (GIXD);[9] for example, an amphiphile consisting of a large cholesterol hydrophobe and a hydrophilic chiral amino acid afforded a crystalline monolayer in which large hydrophobes above the air−water interface encouraged insertion of amino acid molecules from the aqueous subphase (Figure 1d).[10]

Certain Langmuir monolayers have been reported to form self-interdigitated bilayers and multilayers at the air−water interface. Air-stable interdigitated bilayers of 2,3-disubstituted fatty acid methyl esters formed under compression.[11a] Nonamphiphilic cholesterol molecules bearing long alkyl chains formed interdigitated bilayers as a consequence of the large area occluded by the cholesterol moieties at the air−water interface, which created "cavities" into which the alkyl chains of an opposing layer intercalated (Figure 1e).[11b] Crystalline multilayer films with interdigitated chains have been generated upon compression of noncrystalline *p*-pentadecyl-(*R*)-mandelic acid

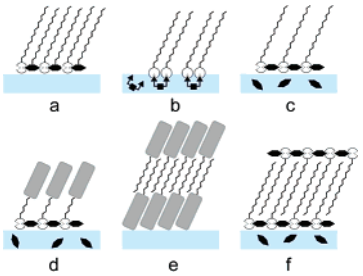

Figure 1. Schematic representations of various Langmuir monolayer architectures: (a) mixed monolayer of amphiphiles assembled through specific interactions at the air−water interface; (b) monolayer of amphiphiles bound through specific interactions to solute guests below the air−water interface; (c) monolayer of amphiphiles bound to water-soluble "guest" molecules at the air−water interface through specific interactions creating an expanded array of hydrophobes; (d) crystalline monolayer of amphiphiles, each equipped with a bulky terminal substituent, assembled with specific interactions with water-soluble molecules at the air−water interface; (e) self-interdigitated crystalline bilayer of nonamphiphilic molecules, equipped with a bulky terminal substituents that proscribe cavities into which the alkyl chains intercalate; (f) bilayer of self-interdigitated monolayers, each with hydrophobes sufficiently expanded through specific binding with water-soluble spacer guest molecules.

* To whom correspondence should be addressed. E-mail: isabelle.weissbuch@weizmann.ac.il; wardx004@umn.edu.
† University of Minnesota.
‡ Risø National Laboratory.
§ The Weizmann Institute of Science.
⊥ Present address: Niels Bohr Institute, University of Copenhagen, Universitetsparken 5, DK-2100 Copenhagen, Denmark.
∥ Present address: Max Planck Institute of Colloids and Interfaces, D-14424 Potsdam, Germany.
▽ Present address: Department of Chemistry, New York University, 31 Washington Place, New York, New York 10003-5180.

10.1021/jp056310r CCC: $33.50
Published on Web 06/30/2006

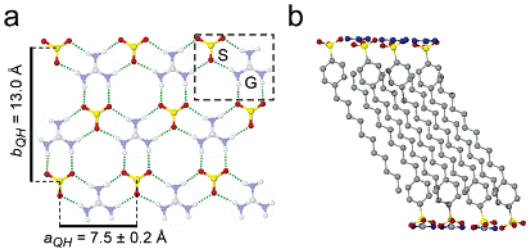

Figure 2. (a) *Quasi*-hexagonal **GS** hydrogen-bonded network observed in crystalline **GS** compounds and expected at the air−water interface for **GS** monolayers. The gray circles represent the regions that are accessible to alkyl chains from an opposing network of the interdigitated bilayer. The area per **GS** formula unit (box) typically is ca. 48 Å^2. (b) Interdigitated bilayer architecture observed in 3D crystals of guanidinium undecylbenzenesulfonate.

monolayers or monolayers consisting of benzoic acid amphiphiles and water-soluble (*R*)-phenylethylamine or *p*-methylbenzylamidinium spacer ions (Figure 1f).[8,12] Collectively, these observations suggest that the judicious selection of amphiphiles or combinations of amphiphiles and complementary hydrophilic "spacer" molecules can permit the formation of expanded crystalline monolayers (i.e., monolayers with a low surface density of hydrophobes), which upon compression could fold to form interdigitated bilayers at the air−water interface.

One of our laboratories has reported numerous three-dimensional (3D) crystalline materials based on a highly persistent two-dimensional (2D) hydrogen-bonded network of guanidinium $C(NH_2)_3^+$ (**G**) ions and sulfonate (**S**) moieties of organomonosulfonate and organodisulfonates.[13−16] The **GS** network, which typically adopts either a "*quasi*-hexagonal" or "shifted ribbon" motif, has been observed in more than 400 compounds derived from various organomonosulfonates and organodisulfonates, usually affording layered architectures. The remarkable persistence of the **GS** network has been attributed to the hydrogen-bonding complementarity of the **G** and **S** ions, the large number of hydrogen bonds within the network (up to six for each **G** and **S** ion), and an inherent structural flexibility of the **GS** sheet, which permits the host frameworks to achieve optimum packing.[17,18] The metrics of the **GS** sheet, in which the **S** sites are separated by 7.2−7.5 Å because of the intervening **G** ions, prescribes voids that permit interdigitation of organic groups from an opposing **GS** sheet, as evident from the solid-state 3D structure of numerous guest-free (**G**)(organomonosulfonates) that crystallize in the discrete bilayer architecture. For example, the amphiphile (**G**)(undecylbenzenesulfonate) crystallizes in a bilayer architecture in which the alkyl substituents of opposing layers interdigitate (Figure 2). This packing motif suggests that monolayers consisting of **G** ions and certain organomonosulfonate amphiphiles would favor the formation of self-interdigitated bilayers at the air−water interface.[19]

We recently reported GIXD studies of crystalline ternary inclusion monolayers at the air−water interface consisting of **G**, 4′-hexadecylbiphenyl-4-sulfonate (C16BPS) and various nonamphiphilic biphenylalkane guests, which were contained between the hydrophobes above the air−water interface.[20] Combined surface pressure−area isotherms and GIXD data revealed a structure-enforcing role for the **GS** network, which stabilized the inclusion monolayers against collapse and loss of guest molecules. Uncompressed guest-free (**G**)C16BPS monolayers were not crystalline, however, even though the compression isotherms revealed signatures of the **GS** network. This indicated that the hydrophobes at the air−water interface were not close packed, presumably because of the large separation introduced by the **G** spacer ion.

Herein we report the characterization, principally by GIXD, of guest-free monolayers formed by octadecylsulfonate amphiphiles, C18S, in the absence and presence of guanidinium ions from the aqueous subphase. Although we reported the (**G**)C18S monolayer previously,[21] its crystal structure was not characterized by GIXD. The GIXD data reported herein reveal that the guest-free (**G**)C18S monolayer is crystalline with highly tilted C18S amphiphiles, which permits the close-packing of the alkyl chains required for crystallinity. Upon compression, this monolayer transforms into two new crystalline phases, one a dense monolayer phase with slightly tilted alkyl chains and disordered sulfonate headgroups and the other a partially ordered, self-interdigitated crystalline multilayer that presumably forms by a "zipper-like" mechanism, similar to that invoked for the transformation of the aforementioned noncrystalline monolayers to interdigitated multilayers (Figure 1f).[8] The GIXD data suggest that the transformation to the multilayer phase is sluggish, which is consistent with kinetic limitations expected for the conversion of a crystalline monolayer to a crystalline multilayer.

Experimental Section

Materials. Sodium octadecylsulfonate (NaC18S) was obtained from Lancaster (UK) and used without further purification. Guanidinium carbonate and sodium carbonate were obtained from Aldrich (Milwaukee, WI) and used without further purification.

Surface pressure−area (π−A) isotherms were recorded on a Nima Langmuir trough (Model No. 611; trough area 10 cm × 30 cm) at a compression rate of 0.5 cm/min (5 cm^2/min) and a subphase temperature of 20.0 ± 0.1 °C. The aqueous subphase was prepared with deionized water (purified to 17.9 Mohm-cm with a Barnstead water purifier) and the selected solute, if any. Surface pressure was recorded with a Wilhelmy balance configured with a paper plate. All monolayers were prepared by the spreading of chloroform solutions of NaC18S (0.4−0.8 mg /mL). An error propagation analysis of the precision of A_{mol} (A_{mol} = the molecular area of the sulfonate amphiphile), based on the trough area and spreading solution concentration, produced an uncertainty in A_{mol} < 0.1 Å^2/sulfonate. Therefore, a conservative value for the uncertainty for A_{mol} would be ±0.5 Å^2/sulfonate.

Grazing incidence X-ray diffraction measurements[22] were performed using the liquid surface diffractometer[22] mounted at the undulator beam line BW1 in HASYLAB at DESY (Hamburg, Germany). A sealed and temperature-controlled Langmuir trough (4 °C), equipped with a Wilhelmy balance for surface pressure measurement of the films, was mounted on the diffractometer. Monochromatic synchrotron radiation (λ = 1.304 Å) was produced by Bragg reflection from a Be crystal. Surface sensitivity was optimized by adjustment of the incident grazing angle (α_i) of the beam, with respect to the water surface, to $\alpha_i = 0.85\alpha_c$ (where $\alpha_c = 0.138°$ is the critical angle for total external reflection of X-rays from the water surface). The footprint of the incident X-ray beam at the air−water interface was 2 mm × 50 mm, and the diffracted radiation was recorded with a one-dimensional position-sensitive detector (PSD), which resolved the vertical component of the X-ray scattering vector, $q_z \cong (2\pi/\lambda) \sin \alpha_f$ (where α_f is the angle between the diffracted beam and the horizon), over the range $0.0 \le q_z \le 1.4$ Å^{-1}. The PSD was mounted vertically behind a horizontally collimating Soller slit with a horizontal resolution width fwhm(q_{xy}) = 0.0084 Å^{-1}. The GIXD patterns were measured by scanning over a range of the horizontal component of the X-ray scattering vector, $q_{xy} \cong (2\pi/\lambda)\,[1 + \cos^2(\alpha_f) - 2\cos(\alpha_f)\cos(2\theta_{xy})]^{1/2}$

(where $2\theta_{xy}$ is the horizontal scattering angle between the beam and the Soller collimator), while simultaneously resolving q_z with the PSD. The GIXD diffraction data can be presented in three ways: (1) as the 2D intensity distribution $I(q_{xy},q_z)$ in a surface or contour plot; (2) as Bragg peaks $I(q_{xy})$ obtained by integrating $I(q_{xy},q_z)$ over q_z; (3) as Bragg rod intensity profiles $I(q_z)$ obtained by integrating $I(q_{xy},q_z)$ over the q_{xy} range corresponding to a specific Bragg peak (after background subtraction).

The unit cell dimensions of the 2D lattice are derived from the q_{xy} positions of the Bragg peaks. The full width at half-maximum of the Bragg peaks (corrected for instrument resolution), fwhm(q_{xy}), gives an estimate of the crystalline coherence lengths $L_{hk} \approx 0.9(2\pi/\text{fwhm}(q_{xy}))$ associated with each h,k reflection. The full width at half-maximum of the Bragg rod intensity profiles, fwhm(q_z), gives a first estimate of the thickness $d \approx 0.9(2\pi/\text{fwhm}(q_z))$ of the 2D crystallites.

Molecular models of 2D crystalline monolayers were constructed using the CERIUS[2] or Molecular Studio computational packages.[23] Least-squares refinement of the structure based on these models and the GIXD data were performed using SHELX-97[24] adapted for 2D crystals.[25,26] Although this software package is designed for 3D single crystals, refinement of a 2D packing arrangement was achieved with the following procedure.[25,26] The continuous Bragg rod intensities distributed along q_z, $|F^2(h,k,q_z)|^2$, were transformed into discrete reflection data sets, $|F(h,k,l)|^2$, wherein a particular Miller index l is associated with a virtual c axis calculated as $c = 2\pi/\Delta q$, where q_z is sampled in very small steps of Δq_z. The superposition of the $|F(h,k,q_z)|^2$ and $|F(-h,-k,q_z)|^2$ Bragg rods, a property of the measured GIXD powder pattern, was simulated in SHELX-97 by imposing a twinning of the crystal about the *ab* plane. Because of the limited amount of diffraction data, refinement was performed with the molecular constituents constrained as rigid bodies, fixed within the measured unit cell dimensions. Following the refinement, the calculated structure factor $|F^2(h,k,l)|$ was converted to a calculated Bragg rod intensity profile $|F(h,k,q_z)|^2$, which was then compared with the experimental data. This comparison allows direct visual inference of the quality of the refined structure.

Atomic Force Microscopy of Deposited Langmuir−Blodgett Films. Multilayer (**G**)C18S films were deposited onto cleaved mica substrates using the Langmuir−Blodgett technique by withdrawing the substrate vertically from an aqueous subphase on which a (**G**)C18S film was prepared. The deposition was performed at a surface pressure of 25 mN/m and an area per molecule below the monolayer collapse point (as determined from the $\pi-A$ isotherm) and a dipping speed of 5 mm/min. The transferred films were imaged in tapping mode with a Nanoscope IIIa Multimode system (Digital Instruments, Santa Barbara, CA), a scanner with a maximum 15 mm scan range, and a 90 mm Si cantilever tip (MikroMasch, Tallinn, Estonia) with an Al coated backside, force constant of 14 N/m and resonant frequency of 270 kHz.

Results and Discussion

Guanidinium-Free Monolayers. Langmuir monolayers of the sodium salt of C18S (NaC18S) on pure water were unstable under compression, as the pressure−area ($\pi-A$) isotherms collapsed at low surface pressures ($\pi \approx 5$ mN/m). The isotherms exhibited a significant dependence on the compression rate, presumably due to kinetic factors associated with dissolution of the NaC18S amphiphile in water. The $\pi-A$ isotherms acquired on aqueous subphases containing 10^{-2} M Na_2CO_3 (Figure 3A) exhibited a pressure lift-off (defined as the area per sulfonate at which pressure begins to increase measurably) at $A_{\text{lift-off}} = 68$ Å^2/sulfonate (a conservative value for the uncertainty in this and subsequent measurements of molecular areas is ±0.5 Å^2/sulfonate; see Experimental Section). This behavior was followed by a gradual increase in the surface pressure with decreasing A_{mol} (A_{mol} is defined as the trough area divided by the number of amphiphile molecules initially spread on the air−water interface). Unlike the behavior observed on pure water, the value of $A_{\text{lift-off}}$ and the shape of the isotherm were independent of the compression rate (in the range 5−20 cm^2/min). The slope of the isotherm began to increase steeply at ca. $A_{\text{mol}} = 30$ Å^2/sulfonate, signaling the formation of a close-packed film. The apparent molecular area, estimated by extrapolation of this rising portion of the isotherm, was ~31 Å^2/sulfonate. The film collapsed at a surface pressure of $\pi = 40.6$ mN/m. These features indicate that excess sodium ions in the aqueous subphase stabilized the NaC18S monolayers at the air−subphase interface, as expected.

Grazing incidence X-ray diffraction (GIXD) was used to determine the 2D packing arrangement of the C18S-based monolayers at the air−water interface. In the absence of compression ($A_{\text{mol}} = 70$ Å^2/sulfonate), NaC18S on aqueous 10^{-2} M Na_2CO_3 did not exhibit diffraction. Compression to $A_{\text{mol}} = 40$ Å^2/sulfonate produced a weak diffraction pattern (not shown) consisting of two broad Bragg peaks associated with a poorly crystalline monolayer and three narrow peaks associated with a multilayer phase. Upon further compression to $A_{\text{mol}} =$ 30 and 25 Å^2/sulfonate, the intensity of the diffraction peaks corresponding to these two phases increased (Figure 3B). The Bragg peaks at $q_{xy} = 1.23$ and 1.41 Å^{-1} were assigned to $\{02\}^{\text{mono}}$ and $\{11\}+\{-11\}^{\text{mono}}$ reflections of the monolayer phase, yielding a rectangular 2D unit cell with $a = 4.95$ Å and $b = 10.2$ Å. The lateral size of the crystallites was only ca. 120 Å, as determined from the fwhm(q_{xy}) of the Bragg peaks. The thickness of the monolayer crystallites was ca. 15 Å, as estimated from the fwhm(q_z) of the corresponding Bragg rods. Based on the q_z positions of the intensity maxima of these Bragg rods (at $q_z = 1.0$ and 0.5 Å^{-1}, respectively), the alkyl chains were tilted with respect to the surface normal by $t = 39.1°$ along the b direction (Scheme 1, $\psi = 90°$). The unit cell, with an area $A_{\text{cell}} = 51$ Å^2, can accommodate two amphiphile molecules tilted along the b direction and related by glide along the b axis, perpendicular to the a axis, which extinguishes the (01) reflection. Although this arrangement would not extinguish the (10) reflection (expected at $q_{xy} = 1.27$ Å^{-1}) on the basis of symmetry considerations, the intensity of this peak may be very weak, owing to the near-centering of one of the amphiphiles, produced by the glide symmetry, in the unit cell. The area per chain, projected on a plane orthogonal to the chains, is $A_{\text{proj}} = A_{\text{cell}}/2 \times \cos(t) = 19.6$ Å^2.

The multilayer phase, which could be distinguished from the coexisting monolayer phase by the fwhm(q_z) of its Bragg rods (corresponding to a thickness of ca. 50 Å), exhibited Bragg peaks at $q_{xy} = 1.335$, 1.355, and 1.48 Å^{-1}. These values can be assigned to $\{11\}^{\text{multi}}$, $\{-11\}^{\text{multi}}$, and $\{02\}^{\text{multi}}$ reflections, respectively, consistent with a near-rectangular unit cell with $a =$ 5.59 Å, $b = 8.49$ Å, and $\gamma = 89.1°$. Like the crystalline monolayer phase, the area of this unit cell, $A_{\text{cell}} = 47.4$ Å^2, can accommodate two amphiphile molecules. The Bragg peaks of this phase are much narrower than those of the monolayer phase, with fwhm(q_{xy}) ≈ 0.01 Å^{-1}, a value consistent with a domain size exceeding 900 Å. In addition, the Bragg rod corresponding to $\{-11\}^{\text{multi}}$ at $q_{xy} = 1.355$ Å^{-1} exhibited two intensity modulations with maxima at q_z values of 0.3 and 0.5 Å^{-1}. On

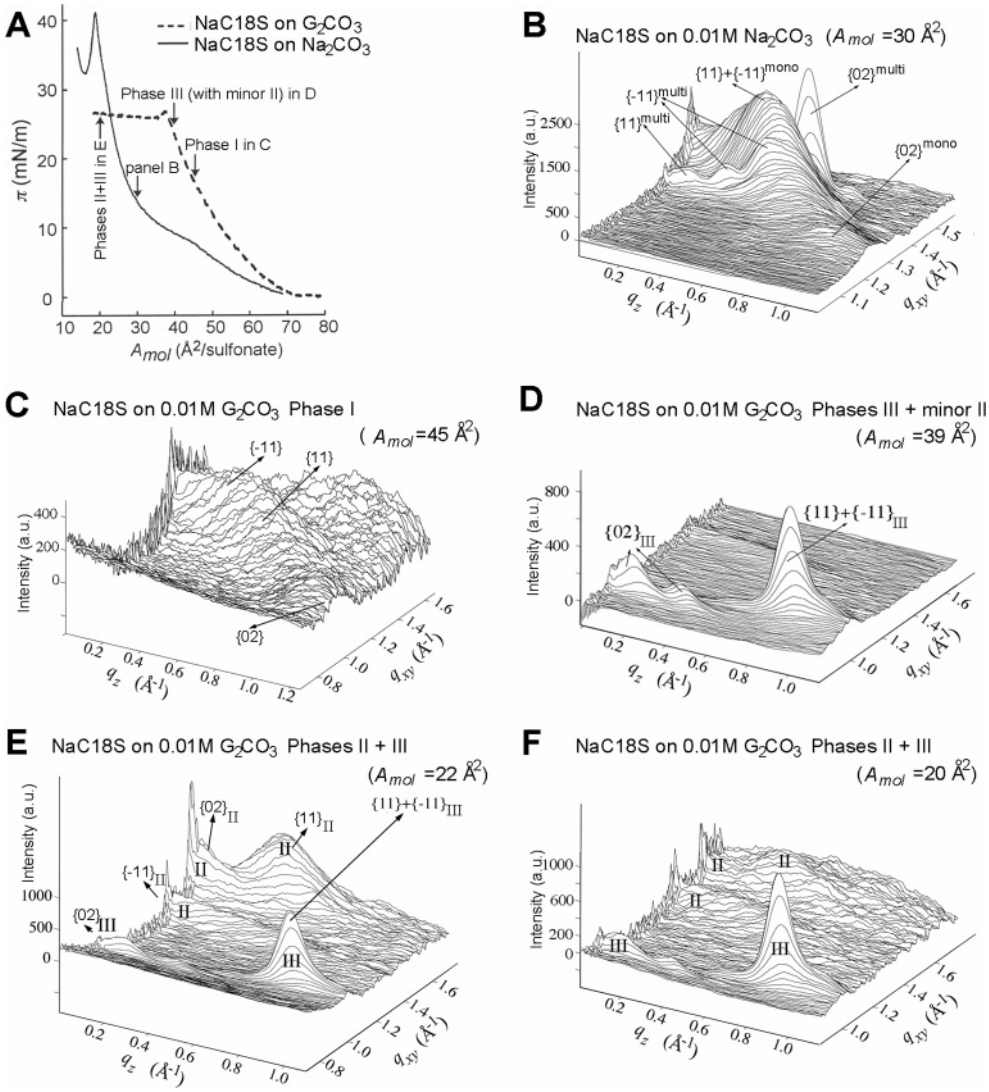

Figure 3. (A) Langmuir surface pressure−area isotherms of NaC18S monolayers on aqueous subphases containing either 0.01 M Na_2CO_3 (solid line) or 0.01 M G_2CO_3 (dashed line). Arrows denote points at which GIXD scans were measured; (B−F) Three-dimensional surface plots of scattered intensity as a function of the horizontal (q_{xy}) and vertical (q_z) components of the scattering vector, $I(q_{xy}, q_z)$, measured at various points indicated by arrows in the isotherms: (B) NaC18S over 0.01 M Na_2CO_3 at A_{mol} = 25 Å^2/sulfonate; (C−F) NaC18S over 0.01 M G_2CO_3 at: (C) A_{mol} = 45 Å^2/sulfonate; (D) A_{mol} = 39 Å^2/sulfonate; (E) A_{mol} = 22 Å^2/sulfonate; (F) A_{mol} = 20 Å^2/sulfonate, collected for a freshly spread monolayer over 0.01 M G_2CO_3, demonstrating the reproducibility of the formation of Phase III.

SCHEME 1

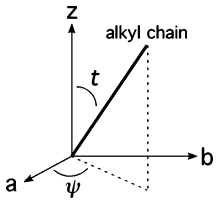

the basis of the Δq_z separation of 0.2 Å^{-1}, the interlayer spacing within this multilayer phase can be estimated as ca. 30 Å, consistent with the multilayer comprising two noninterdigitated layers. The appearance of this multilayer phase upon compression at A_{mol} = 40 Å^2/sulfonate is surprising, as the NaC18S monolayer should not yet have covered the surface fully under these conditions. The multilayer peaks do not correspond to any of the peaks observed in the powder X-ray diffraction pattern of pure NaC18S, which argues against the presence of microcrystals in the spreading solution.

Guanidinium-Containing Monolayers. The $\pi-A_{mol}$ isotherm measured for NaC18S spread on 10^{-2} M aqueous guanidinium carbonate (G_2CO_3) exhibited a lift-off area of $A_{lift-off}$ = 71 Å^2/sulfonate (Figure 3A). The isotherm rose rapidly as the monolayer was compressed and extrapolation of the rising portion afforded an apparent area per molecule of ∼55.5 Å^2/sulfonate, which was substantially larger than the value of 31 Å^2/sulfonate measured in the absence of **G** ions (see above). The film collapsed at a surface pressure of π = 27 mN/m, followed by a plateau region that persisted to low molecular areas (A_{mol} = 15 Å^2/sulfonate).

GIXD measurements of this (**G**)C18S monolayer at A_{mol} = 45−50 Å^2/sulfonate (denoted Phase I), where substantial separation between hydrophobes would be expected (Figure 3C), revealed relatively weak and broad Bragg peaks, signaling poor crystallinity. Nonetheless, the maxima of the Bragg peaks could be distinguished, with q_{xy} = 0.97, 1.38, and 1.40 Å^{-1}. These reflections can be assigned Miller indices $\{01\}_o$, $\{-11\}_o$, and $\{10\}_o$, yielding a primitive oblique unit cell with a_o = 4.83 Å, b_o = 6.96 Å, γ_o = 111.5° and A_{cell} = 31.2 Å^2. For purposes of comparison with the NaC18S monolayer on Na_2CO_3, this unit cell was transformed ($\boldsymbol{a}_r = \boldsymbol{a}_o$, $\boldsymbol{b}_r = \boldsymbol{a}_o + 2\boldsymbol{b}_o$) into a near-rectangular unit cell with a_r = 4.82 Å, b_r = 12.96 Å, γ_r = 88.7°

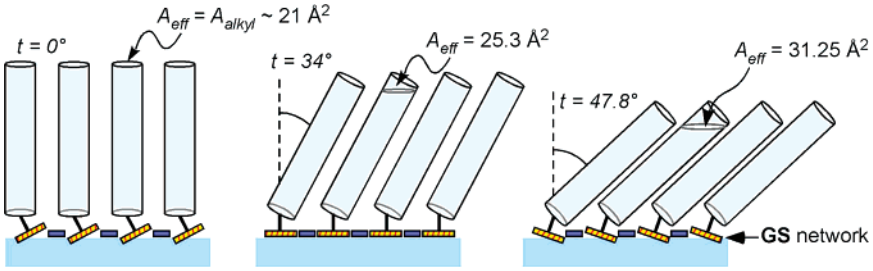

Figure 4. Schematic representation of a GC18S monolayer at the air−water interface (alkyl chains portrayed as gray cylinders, sulfonate headgroups as yellow rectangles, **G** ion spacers as blue rectangles). (Left) Vertical orientation of all-trans alkyl chains requires tilting of the sulfonate headgroups out of the plane of the air−water interface. In the presence of **G** ion spacers, the chains are unable to achieve close packing because the cross-sectional area ($A_{alkyl} \approx 21$ Å^2) of the alkyl chain is less than the separation between sulfonate headgroups. (Center) All-trans alkyl chains in monolayers with sulfonate headgroups aligned parallel to the air−water interface are naturally tilted by $t = 34°$, but this is insufficient for close packing. (Right) Close packing can be achieved at an angle $t = 47.8°$, which requires the sulfonate headgroups to rotate out of the plane of the air−water interface. This value of t corresponds to an effective area per alkyl chain (A_{eff}, the area of the chain projected onto the air−water interface) of 31.25 Å^2. These values of t and A_{eff} agree with those determined by GIXD for the Phase I monolayer, signifying close-packed alkyl chains.

and $A_{cell} = 62.5$ Å^2, for which the three reflections of the primitive oblique unit cell transform to $\{02\}_r$, $\{11\}_r$, and $\{-11\}_r$, respectively. This unit cell is substantially different from that obtained for the NaC18S monolayer, signifying a structure-directing role for the **G** ion, presumably through hydrogen bonding with the sulfonate groups at the air−water interface. The film thickness, estimated from the fwhm(q_z) of the Bragg rods, is ca. 15 Å, consistent with the formation of a crystalline monolayer containing highly tilted C18S amphiphile chains. Based on the q_z positions of the maxima of the Bragg rod intensity profiles (at 1.12, 0.66, and 0.46 Å^{-1}; Figure 3C), the tilt angle and tilt direction of the alkyl chains were $t = 49°$ and $\psi = 85°$ (Scheme 1).

The unit cell area of Phase I ($A_{cell} = 62.5$ Å^2) can accommodate 2 amphiphile molecules with an effective area *per* chain of $A_{eff} = A_{cell}/2 = 31.25$ Å^2 projected onto the air−water interface. This would correspond to an actual chain cross-sectional area of $A_{alkyl} = A_{cell}/2 \times \cos 49° = 20.4$ Å^2, similar to the value of $A_{alkyl} \approx 21$ Å^2 often accepted for an alkyl chain. $A_{cell}/2$ is less than the A_{mol} value at which these data was collected, most likely signaling a heterogeneous monolayer consisting of crystalline domains of Phase I interspersed with noncrystalline regions. If the all-trans chains were exactly perpendicular to the air−water interface ($t = 0$), the sulfonate groups would need to rotate out of the plane of the GS sheet, and the effective area per chain would be $A_{eff} = A_{alkyl} \approx 21$ Å^2 (Figure 4). If the sulfonate groups of the (**G**)C18S monolayer—with a quasihexagonal GS network at the air−water interface—were strictly parallel with the air−water interface and if the alkyl chains retained the all-trans configuration, the chain tilt would be $t = 34°$ and the effective area of the alkyl chain projected onto the air−water interface would be $A_{eff} = 25.3$ Å^2, based on an actual alkyl chain area of $A_{alkyl} = 21$ Å^2. Under these conditions, the surface density of the alkyl chains would be less than that required for close-packing, as the area available to each organosulfonate group in an ideal flat **GS** sheet is ca. 48 Å^2 due to the G ion spacer (see Figure 2). For an all-trans alkane chain to achieve a value of $A_{eff} = 48$ Å^2, the chain tilt would need to be $t = 64°$, which would require substantial rotation of the sulfonate group out of the plane of the air−water interface (not shown in Figure 4). Notably, molecular models reveal that if $A_{eff} = 31.25$ Å^2 ($A_{cell}/2$ for Phase I) close packing can be achieved at a tilt angle of $t = 47.8°$, the experimentally observed value. This clearly suggests that Phase I adopts a structure that permits close packing of the alkyl chains,[27] as required for crystallization, but with some rotation of the sulfonate groups out of the plane of the air−water interface that perturbs the ideal structure of the quasi-hexagonal **GS** network.

These results are particularly interesting because GIXD measurements performed on monolayers of hexadecylbiphenylsulfonic acid (C16BPSA) on a 10^{-2} M G_2CO_3 aqueous subphase did not detect a crystalline monolayer, whether compressed or uncompressed.[20] Instead, the surface pressure−area isotherms and GIXD indicated formation of a close-packed monolayer in which the **G** ions were forced out of the plane of the sulfonate groups upon compression. The formation of a crystalline (**G**)C18S monolayer with **G** ion spacers suggests that the C18S chains, lacking the rigid biphenyl group, are more capable of adopting conformations that permit substantial tilt of the hydrophobes so that close-packing can be achieved.

Upon compression of the (**G**)C18S monolayer to the plateau at $A_{mol} = 39$ Å^2/sulfonate, the peaks associated with Phase I disappeared and new peaks emerged that were assignable to two new coexisting crystalline phases, denoted Phase II and Phase III (Figure 3D). The peaks associated with each phase could be distinguished by their relative changes in intensity as the film was compressed. At this surface pressure, the single peak associated with Phase II was quite small but detectable. When the same monolayer was compressed further to $A_{mol} = 22$ Å^2/sulfonate, the intensity of the peaks assigned to both Phase II and Phase III increased, particularly the intensity of Phase II (Figure 3E). The formation of both phases was reproducible, as evidenced by GIXD measurements performed on new films under the same conditions (Figure 3F). Although the number of trials was limited due to the constraints of synchrotron beam time, the relative amounts of each phase, as deduced from the peak intensities, appeared to depend on the compression sequence used. The sequence represented by the data in Figure 3C−E was collected over a period of approximately 4 h, first by (1) gradual compression to $A_{mol} = 60$ Å^2/sulfonate followed by a 10 min of data acquisition (not shown, negligible diffraction), (2) compression to $A_{mol} = 50$ Å^2/sulfonate followed by 60 min of data acquisition (not shown), (3) compression to $A_{mol} = 45$ Å^2/sulfonate followed by 45 min of data acquisition (Figure 3C), (4) compression to $A_{mol} = 39$ Å^2/sulfonate followed by 60 min of data acquisition (Figure 3D), and (5) compression to $A_{mol} = 22$ Å^2/sulfonate followed by 45 min of data acquisition (Figure 3E). The data in Figure 3F was collected over a similar time period. In a separate experiment in which another (**G**)C18S film was compressed stepwise but with rapid scans at each pressure ($A_{mol} = 70 \rightarrow 42 \rightarrow 27 \rightarrow 16$ Å^2/sulfonate; approximately 10 min at each surface pressure), Phase I was retained and Phases II and III were not observed. Collectively,

these data suggest that the formation of Phases II and III is complex and kinetically limited under the conditions employed here.

Phase II of (**G**)C18S exhibits three relatively broad Bragg rods at $q_{xy} = 1.45$, 1.63, and 1.66 Å^{-1} with maximum intensity at q_z values of ∼0.4, 0, and ∼0.4 Å^{-1}, respectively (Figure 3E, F). These peaks were assigned as {1,0}, {−11}, and {01}, corresponding to an oblique unit cell with $a_o = 4.87$ Å, $b_o = 4.26$ Å, $\gamma_o = 117.21°$, and $A_{cell} = 18.44$ Å^2. For comparison with Phase I, this unit cell was transformed ($\boldsymbol{a}_r = \boldsymbol{a}_o + \boldsymbol{b}_o$, $\boldsymbol{b}_r = -\boldsymbol{a}_o + \boldsymbol{b}_o$) into a unit cell with $a_r = 4.78$ Å, $b_r = 7.80$ Å, $\gamma_r = 98.67°$, and $A_{cell} = 36.88$ Å^2, for which the three reflections of the primitive unit cell transform to $\{-11\}_r$, $\{02\}_r$, and $\{11\}_r$, respectively. This unit cell, which is far from being rectangular, contains 2 amphiphile molecules tilted by $t = 17°$ from the normal to the surface along the *a* axis, as derived from the q_z values of the maximum intensity of the three Bragg rods. On the basis of this tilt direction, the alkyl chains are presumably related by pseudo-glide symmetry. The cross-sectional area per amphiphile, however, is $A_{alkyl} = 17.6$ Å^2 (36.88/2 × cos 17° = 17.6 Å^2), which is much smaller than the 48 Å^2 area occupied by one C18S amphiphile and an accompanying **G** ion. This value also is smaller than the smallest $A_{alkyl} = 18.4$ Å^2 of alkyl chains in low-temperature structures.[27] We note, however, that A_{alkyl} values of 18.0, 17.9, and 17.6 Å^2 were reported for the crystalline monolayer phases of long-chain alcohol derivatives of 1,3-bis(ethynylenebenzene) molecules adopting an inverted U-shape.[28,29] The film thickness, estimated from the fwhm(q_z) of the Bragg rods, is ∼19 Å, consistent with the formation of a new crystalline monolayer different from the Phase I observed at low surface coverage. This 19 Å film thickness is also smaller than that expected based on the observed tilt angle and the calculated length of the C18 alkyl chain only ((17× 1.265 Å + 1.12 Å) × cos 17° = 21.6 Å), that is, if the sulfonate headgroup is ignored. This value can only be explained by a monolayer organization in which the **G** ions were forced beneath the sulfonate groups and both are disordered, such that they do not contribute to diffraction.

The strong and relatively narrow Bragg rods at $q_{xy} = 0.97$ and 1.03 Å^{-1} were assigned to Phase III of (**G**)C18S (Figure 3D − F). The Bragg rod at $q_{xy} = 1.03$ Å^{-1} exhibits a single intensity maximum at $q_z = 0.83$ Å^{-1}, whereas $q_{xy} = 0.97$ Å^{-1} displays two modulations with maximum intensity at $q_z = 0.13$ and 0.36 Å^{-1} (Figure 3D−F). The q_{xy} peaks could be indexed to either of two rectangular unit cells: $a = 6.91$ Å, $b = 12.96$ Å, and $A_{cell} = 89.6$ Å^2 (assignment 1: $q_{xy} = 0.97$ and 1.03 Å^{-1}, corresponding to {02} and superimposed {11} + {−11} reflections, respectively) or $a = 7.64$ Å, $b = 12.2$ Å, and $A_{cell} = 93.3$ Å^2 (assignment 2, with the reverse order). It is expected for a rectangular unit cell that the intensity of the superimposed {11} + {−11} reflections would be larger than that of the {02} reflection; therefore, assignment 1 was regarded as more likely. The unit cell ($A_{cell} = 89.6$ Å^2) can accommodate 4 molecules. The film thickness of ∼40 Å, as estimated from the fwhm(q_z) of the Bragg rods, combined with the double intensity modulation of the {02} Bragg rod, suggested that Phase III was an unusual example of an interdigitated multilayer generated upon compression of the highly tilted monolayer Phase I.

An initial model of the packing arrangement of Phase III was constructed based on the 2D unit cell parameters calculated from the q_{xy} data using CERIUS^2 software.[23] This model consisted of four C18S amphiphiles per unit cell, two projecting from the **GS** sheet at the air−water interface and the remaining two projecting from an opposing **GS** sheet, generating a single

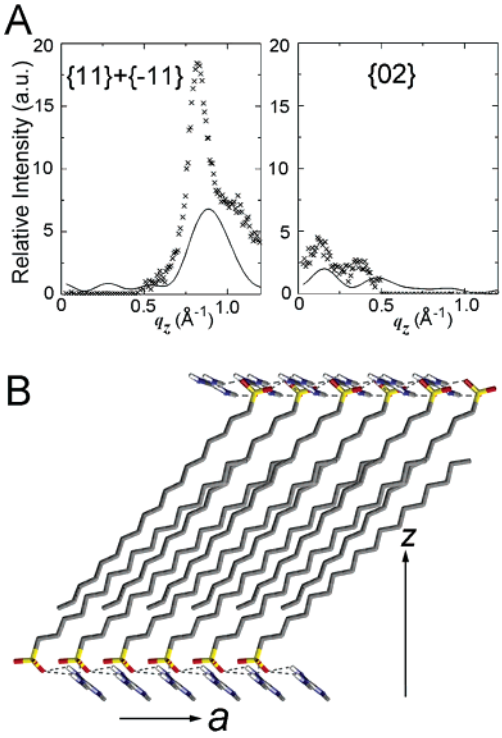

Figure 5. (A) Calculated (solid line) and experimental (points) Bragg rod intensity profiles for the single bilayer model of crystalline (G)-C18S Phase III formed by compression at $A_{mol} = 39$ Å^2/sulfonate (plateau of the isotherm in Figure 3A); (B) Corresponding 2D packing arrangement, as viewed parallel to the water surface along the *b* axis. This arrangement is similar to the architecture pictured in Figure 1f. Only the carbon atoms of the alkyl chains are depicted. Guanidinium ions are drawn as blue, oxygen and sulfur atoms as red and yellow, respectively, and the alkyl chains as black.

interdigitated bilayer similar to that depicted in Figure 1f. The model was constructed from two independent but *pseudo*-glide related (**G**)C18S molecules, similar to those in the 3D crystal of (**G**)C4S,[13] which by pseudo-centering complete the 2D packing arrangement. According to the position at $q_z = 0.83$ Å^{-1} of the intensity maximum of the {11} + {−11} Bragg rod, we assumed that the amphiphile chains were tilted by ∼39° along the *a* axis of the unit cell, yielding a layer thickness of ∼26 Å. This model was refined by X-ray structure factor calculations using the SHELX97 program[24] adapted for 2D structures,[25,26] with the molecules constrained as rigid bodies. The refined packing arrangement (Figure 5B) produces an intensity maximum of the {11} + {−11} Bragg rod at $q_z \approx 0.85$ Å^{-1} and two intensity modulations of the weak {02} Bragg rod (Figure 5A). The fwhm(q_z) of the calculated {11} + {−11} Bragg rod, however, was much larger than the experimental value, indicating that the film contains more than one interdigitated bilayer. Indeed, when a partially ordered second interdigitated layer was added to the model, the structure factor calculations produced an improved, although not very good, fit to the Bragg rod intensity profiles (Figure 6A).

The packing arrangement of this interdigitated multilayer is illustrated in Figure 6B,C, as viewed parallel to the water surface along both *a* and *b* axes, respectively. The refined 2D packing arrangement afforded a layer thickness of ∼40 Å, in agreement with the experimental value estimated from the fwhm(q_z). The multilayer consists of one ordered **GS** sheet at the bottom in contact with the air−water interface, two ordered **GS** sheets in the center, and a top layer consisting presumably of a disordered **GS** sheet and partially disordered alkyl chains. Tapping-mode atomic force microscope (TMAFM) images of a (**G**)C18S film

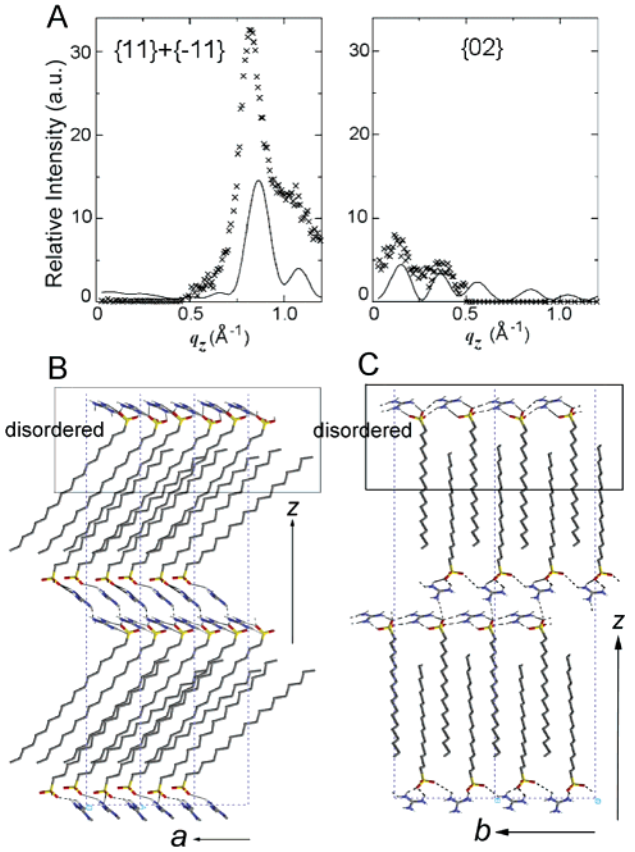

Figure 6. (A) Calculated (solid line) and experimental (points) Bragg rod intensity profiles for the partially ordered multilayer model of crystalline (**G**)C18S Phase III formed by compression at A_{mol} = 39 Å^2/sulfonate (plateau of the isotherm in Figure 3A); (B, C) Corresponding 2D packing arrangement, as viewed parallel to the water surface along the *b* and *a* axes. Only the carbon atoms of the alkyl chains are depicted. Guanidinium ions are drawn as blue, oxygen and sulfur atoms as red and yellow, respectively, and the alkyl chains as black.

that had been transferred to a cleaved mica substrate at A_{mol} = 25 Å^2/sulfonate exhibited steps that could be attributed to interdigitated multilayers (see Supporting Information, Figure S1). The average step height measured by AFM was 30 Å, in close agreement with the layer thickness obtained in the refined packing arrangement of Phase III.

The formation of the interdigitated (**G**)C18S layers may occur by a "zipperlike" folding in which the **G** ion behaves as a spacer molecule that maintains the spacing between hydrophobes required for interdigitation during the transformation of Phase I. This process appears somewhat similar to the interdigitated multilayers generated upon compression of an amorphous monolayer of *p*-pentadecylbenzoic acid and water-soluble *p*-methyl-benzamidinium ions.[8] The (G)C18S monolayer, however, is crystalline, requiring the interdigitation of two crystalline layers during the transformation of Phase I to Phase III. The formation of the interdigitated layer structure in the horizontal plateau region of the $\pi-A$ isotherm (Figure 3A) was dependent upon the compression rate, with the interdigitated (**G**)C18S multilayer obtained only when the monolayer was compressed in small steps up to and through the collapse point of the isotherm. In contrast, the interdigitated multilayer did not form when the (**G**)C18S film was compressed rapidly, even if it was compressed to A_{mol} = 16 Å^2/sulfonate. This behavior suggests kinetic limitations for the "zipperlike" transformation from the crystalline monolayer Phase I to the crystalline interdigitated multilayer Phase III, possibly reflecting slow dynamics of the chain reorganization of the crystalline monolayer precursor that would be required for interdigitation.

Conclusion

NaC18S amphiphiles self-assemble into crystalline monolayers when spread on aqueous subphases containing **G** ions, a phenomenon not observed previously for related binary monolayers. The formation of crystalline (**G**)C18S monolayers, with **G** ion spacers that separate the amphiphile molecules, is attributed to the ability of the alkyl chains of the C18S amphiphiles to tilt substantially so that close-packing of the amphiphile hydrophobes can be realized. **GS** intermolecular hydrogen-bonding in the (**G**)C18S monolayer combined with close-packing of alkane chains stabilized the crystalline expanded monolayer, even in uncompressed form, up to its collapse point. Further compression resulted in the formation of a crystalline self-interdigitated multilayer reminiscent of those observed upon the collapse of certain amorphous expanded monolayers. The formation of the (**G**)C18S self-interdigitated layers was dependent on the history of the sample and the rate of compression, suggesting sluggish kinetics for the chain reorganization during the zipperlike assembly of the crystalline interdigitated layer from the crystalline monolayer.

Acknowledgment. This work was supported by the National Science Foundation (DMR-0305278), the MRSEC Program of the National Science Foundation (DMR-0212302), the United States-Israel Binational Science Foundation (BSF), the Carlsberg Foundation, the DanSync Programme of the Danish Natural Science Research Council, and by the European Community-Research Infrastructure Action under the FP6 "Structuring the European Research Area" Program (through the Integrated Infrastructure Initiative "Integrating Activity on Synchrotron and Free Electron Laser Science"). S.M.M. gratefully acknowledges the financial support of a Sundahl Fellowship.

Supporting Information Available: SHELX-97 files (.res, .hkl, .fcf, .lst, all in .txt format) and tapping mode atomic force microscopy image of the (G)C18S multilayer. This material is available free of charge via the Internet at http://pubs.acs.org.

References and Notes

(1) Kuzmenko, K.; Kjaer, K.; Als-Nielsen, J.; Lahav, M.; Leiserowitz, L. *J. Am. Chem. Soc.* **1999**, *121*, 2657.

(2) Gidalevitz, D.; Weissbuch, I.; Kjaer, K.; Als-Nielsen, J.; Leiserowitz, L. *J. Am. Chem. Soc.* **1994**, *116*, 3271.

(3) Bohanon, T. M.; Denziger, S.; Fink, R.; Paulus, W.; Ringsdorf, H.; Weck, M. *Angew. Chem., Int. Ed. Engl.* **1995**, *34*, 58.

(4) (a) Ariga, K.; Kunitake, T. *Acc. Chem. Res.* **1998**, *31*, 371. (b) Cha, X.; Ariga, K.; Kunitake T. *J. Am. Chem. Soc.* **1996**, *118*, 9545. (c) Sasaki, D. Y.; Kurihara, K.; Kunitake T. *J. Am. Chem. Soc.* **1992**, *114*, 10994.

(5) Siegel, S.; Kindermann, M.; Regenbrecht, M.; Vollhardt, D.; von Kiedrowski, G. *Prog. Colloid Polym. Sci.* **2000**, *115*, 233.

(6) Plaut, D. J.; Lund, K. M.; Ward, M. D. *Chem. Comm.* **2000**, *9*, 769.

(7) Tyson, J. C.; Moore, J. L.; Hughes, K. D.; Collard, D. M. *Langmuir* **1997**, *13*, 2068.

(8) Kuzmenko, I.; Kindermann, M.; Kjaer, K.; Howes, P. B.; Als-Nielsen, J.; Granek, R.; von Kiedrowski, G.; Leiserowitz, L.; Lahav, M. *J. Am. Chem. Soc.* **2001**, *123*, 3771.

(9) Kuzmenko, I.; Rapaport, H.; Kjaer, K.; Als-Nielsen, J.; Weissbuch, I.; Lahav, M.; Leiserowitz, L. *Chem. Rev.* **2001**, *101*, 1659.

(10) Alonso, C.; Eliash, R.; Jensen, T. R.; Kjaer, K.; Lahav, M.; Leiserowitz, L. *J. Am. Chem. Soc.* **2001**, *123*, 10105.

(11) (a) Chen, X.; Wiehle, S.; Weygand, M.; Brezesinski, G.; Klenz, U.; Galla, H.-J.; Fuchs, H.; Haufe, G.; Chi, L. *J. Phys. Chem. B.* **2005**, *109*, 19866. (b) Alonso, C.; Kuzmenko, I.; Jensen, T. R.; Kjaer, K.; Lahav, M.; Leiserowitz, L. *J. Phys. Chem. B* **2001**, *105*, 8563.

(12) Kuzmenko, I.; Buller, R.; Bouman, W. G.; Kjaer, K.; Als-Nielsen, J.; Lahav, M.; Leiserovitz, L. *Science* **1996**, *274*, 2046.
(13) Russell, V. A.; Etter, M. C.; Ward, M. D. *J. Am. Chem. Soc*. **1994**, *116*, 1941.
(14) Swift, J. A.; Pivovar, A. M.; Reynolds, A. M. *J. Am. Chem. Soc*. **1998**, *24*, 5887.
(15) Evans, C. C.; Sukarto L.; Ward, M. D. *J. Am. Chem. Soc*. **1999**, *121*, 320.
(16) Holman, K. T.; Pivovar, A. M.; Ward, M. D. *Science* **2001**, *294*, 1907.
(17) Holman K. T.; Ward, M. D. *Angew. Chem., Int. Ed.* **2000**, *39*, 1653.
(18) Holman, K. T.; Martin, S. M.; Parker, D. P.; Ward, M. D. *J. Am. Chem. Soc.* **2002**, *123*, 4421.
(19) Martin, S. M.; Yonezawa, J.; Horner, M. J.; Macosko, C. W.; Ward, M. D. *Chem. Mater*. **2004**, *16*, 3045.
(20) Plaut, D. J.; Martin, S. M.; Kjaer, K.; Weygand, M. J.; Leiserowitz, L.; Lahav, M.; Weissbuch, I.; Ward, M. D. *J. Am. Chem. Soc*. **2003**, *125*, 15922.
(21) Frostman, L. M.; Ward, M. D. *Langmuir* **1994**, *10*, 576.
(22) Jensen, T. R.; Kjaer, K. Structural Properties and Interactions of Thin Films at the Air−Liquid Interface Explored by Synchrotron X-ray Scattering. In: *Novel Methods to Study Interfacial Layers*; Möbius, D., Miller, R., Eds.; Studies in Interface Science, Vol. 11; Elsevier Science: Amsterdam, 2001; pp 205−254.
(23) CERIUS^2 (IRIX platform) and Materials Studio (Windows platform) computational packages, Accelrys, San Diego, CA.
(24) Sheldrick, G. M. *SHELX-97: Program for Crystal Structure Determination*; University of Göttingen: Gottingen, Germany, 1997.
(25) Weissbuch, I.; Baxter, P. N. W.; Kuzmenko, I.; Cohen, H.; Cohen, S.; Kjaer, K.; Howes, P. B.; Als-Nielsen, J.; Lehn, J.-M.; Leiserowitz, L.; Lahav, M. *Chem.−Eur. J.* **2000**, *6*, 725.
(26) Rapaport, H.; Kuzmenko, I.; Lafont, S.; Kjaer, K.; Howes, P. B.; Als-Nielsen, J.; Lahav, M.; Leiserowitz, L. *Biophys. J.* **2001**, *81*, 2729.
(27) Kuzmenko, I.; Kaganer, M.; Leiserowitz, L. *Langmuir* **1998**, *14*, 3882.
(28) Lederer, K.; Godt, A.; Howes, P. B.; Kjaer, K.; Als-Nielsen, J.; Lahav, M.; Wegner, G.; Leiserowitz, L.; Weissbuch, I. *Chem.−Eur. J.* **2000**, *6*, 2173.
(29) Weissbuch, I.; Lahav, M.; Leiserowitz, L.; Lederer, K.; Godt, A.; Wegner, G.; Howes, P. B.; Kjaer, K.; Als-Nielsen, *J. Phys. Chem.* **1998**, *102*, 6313.